ELSEVIER

Chemical Engineering Journal 127 (2007) 31–38

Chemical Engineering Journal

www.elsevier.com/locate/cej

Reactivity of high surface area CeO_2 synthesized by surfactant-assisted method to ethanol decomposition with and without steam

N. Laosiripojana [a,*], W. Sutthisripok [b], S. Assabumrungrat [c]

[a] *The Joint Graduate School of Energy and Environment, King Mongkut's University of Technology Thonburi, Bangkok 10140, Thailand*
[b] *Department of Mining and Materials Engineering, Faculty of Engineering, Prince of Songkla University, Songkla, Thailand*
[c] *Center of Excellence in Catalysis and Catalytic Reaction Engineering, Department of Chemical Engineering, Faculty of Engineering, Chulalongkorn University, Bangkok 10330, Thailand*

Received 11 October 2005; received in revised form 5 September 2006; accepted 22 September 2006

Abstract

High surface area CeO_2 (CeO_2 (HSA)) synthesized by surfactant-assisted method was found to have useful ethanol decomposition activity producing H_2, CO, CO_2, and CH_4 even when operated without the presence of steam. The catalyst provides high resistance toward carbon deposition compared to Ni/Al_2O_3 and the conventional low surface area CeO_2 (CeO_2 (LSA)). The reactivity toward ethanol decomposition for CeO_2 is due to its high oxygen storage capacity (OSC). During the decomposition process, the gas–solid reactions between the gaseous components, which are homogenously generated from the ethanol decomposition, i.e. C_2H_6, C_2H_4, CH_4, CO_2, CO, H_2O, and H_2, and the lattice oxygen ($O_O{}^x$) on CeO_2 surface take place. The reactions of surface adsorbed hydrocarbons with the lattice oxygen ($C_nH_m + O_O{}^x \rightarrow nCO + m/2(H_2) + V_O{}^{\bullet\bullet} + 2e'$) can produce synthesis gas (CO and H_2) and prevent the formation of carbon species from hydrocarbon decomposition reactions ($C_nH_m \rightarrow nC + m/2H_2$).

In particular, it was observed that the ethanol decomposition rate over CeO_2 (HSA) is proportional to the inlet ethanol partial pressure but independent of the inlet steam partial pressure. This result suggests that the rate of ethanol decomposition is governed by the slow reaction of adsorbed ethanol or surface hydrocarbon species with lattice oxygen in CeO_2, and a rapid gas–solid reaction between oxygen source in the system and the reduced ceria to replenish the oxygen.

Keywords: Ethanol; Internal reforming; Hydrogen; SOFC; CeO_2

1. Introduction

Hydrogen is expected to be one of the most promising fuels in the near future. It could be produced efficiently from the catalytic reforming of several fuels such as methane, methanol, bio-ethanol, gasoline and other oil derivatives. According to the current oil crisis and the shortage of fossil fuels, the development of the biomass-based fuels attracts much attention. Among renewable resources, bio-ethanol is a promising candidate for converting to hydrogen-rich gas, since it is readily produced from renewable resources (e.g. fermentation of biomasses) and has reasonably high hydrogen content [1,2].

Previously, the reforming of ethanol has been studied by several researchers [3–23]. Most of them reported that the major difficulty to reform ethanol is the possible degradation of the catalyst due to the carbon deposition. Therefore, most of the recent works on the reforming of ethanol have been based on the noble metal catalysts (e.g. Rh, Ru, Pt, Pd) over several oxide supports (e.g. Al_2O_3, MgO, SiO_2, TiO_2) [7,9,10,12,20–22], as these precious metals were reported to provide high resistance to the carbon formation compared to the conventional catalysts (i.e. Ni based catalyst). Nevertheless, the current prices of these metals are very high for commercial uses, and the availability of some precious metals such as ruthenium was too low to have a major impact on the total reforming catalyst market [24].

The present work is aimed at the development of an alternative catalyst that is cheaper than the noble metal materials and enables to decompose ethanol with high resistance toward carbon deposition. It is well established that cerium oxide (CeO_2) is used as a catalyst in a wide variety of reactions involving oxidation, or partial oxidation, of hydrocarbons (e.g. automotive catalysis) [25,26]. This material contains a high concentration of highly mobile oxygen vacancies, which act as a local source or sink for oxygen involved in reactions taking place on the surface

* Corresponding author. Tel.: +662 8729014; fax: +662 8726736.
E-mail address: navadol_l@jgsee.kmutt.ac.th (N. Laosiripojana).

1385-8947/$ – see front matter © 2006 Elsevier B.V. All rights reserved.
doi:10.1016/j.cej.2006.09.020

[27–33]. There is now increasing interest in using ceria in more reducing conditions, such as in methane reforming at the anodes of solid oxide fuel cells (SOFC), where the potential deactivation through carbon deposition is much greater [34,35]. Importantly, at the temperature above 700 °C, the gas–solid reaction between CeO_2 and CH_4 produces synthesis gas with a H_2/CO ratio of two. The major limitation to apply ceria for high temperature applications is its low specific surface area due to the significant size reduction by thermal sintering [36]. Therefore, the use of high surface area (HSA) ceria would be a good procedure to improve its catalytic performance at high operating temperatures. Several methods have recently been described for the preparation of CeO_2 (HSA) solid solution. Among these methods, the surfactant-assisted approach was employed to prepare high surface area CeO_2 with improved textural, structural, and chemical properties [36]. Our previous publication [37] also presented the achievement of CeO_2 with high surface area and good stability after thermal treatment by this preparation method.

In this work, high surface area CeO_2 (CeO_2 (HSA)) was first synthesized by the surfactant-assisted method. The reactivity toward decomposition of ethanol, the effect of inlet steam content, and the resistance toward carbon formation of this material were investigated at 700–1000 °C, compared to those of conventional CeO_2 (CeO_2 (LSA)) prepared by precipitation method and Ni/Al_2O_3. At steady state, the influences of temperature and inlet components on the product selectivities from the decomposition of ethanol over CeO_2 (HSA) were then determined. At the end of this article, the gas–solid redox mechanism between the hydrocarbons present in the system and the lattice oxygen (O_O^x) on the surface of CeO_2 (HSA) was discussed.

2. Experimental

2.1. Catalyst preparation and characterization

CeO_2 (HSA) was prepared by mixing an aqueous solution of 0.1 M cetyltrimethylammonium bromide solution (Aldrich), to a 0.1 M cerium chloride. The molar ratio of ([Ce])/[cetyltrimethylammonium bromide] was kept constant at 0.8. The mixture was stirred and then aqueous ammonia was slowly added at a constant rate of 0.165 $cm^3\ min^{-1}$ until the pH was 11.5. The mixture was then sealed and placed in a thermostatic bath maintained at 90 °C for 3 days. After that, the mixture was cooled and the resulting precipitate was filtered and washed repeatedly with water and appropriate solvent. It was dried overnight in an oven at 110 °C, and then calcined in air for 6 h.

CeO_2 (LSA) was prepared by the conventional precipitation of cerium chloride. The starting solution was prepared by mixing 0.1 M of this metal salt solution with 0.4 M of ammonia at a 2:1 volumetric ratio. The filtered powder was then treated under the same procedures as CeO_2 (HSA). BET measurements of CeO_2 (both LSA and HSA) were carried out at different calcination temperatures in order to determine the change in specific surface area due to the thermal sintering. As presented in Fig. 1, after drying, surface areas of 308 and 55 $m^2\ g^{-1}$ were observed for CeO_2 (HSA) and conventional CeO_2, respectively and, as expected, the surface area dramatically decreased at high calcination temperatures. However, the value for CeO_2 (HSA) is still appreciable after calcination at 1000 °C. The redox properties and redox reversibilities of these calcined CeO_2 (both LSA and HSA) were then determined by the temperature-programmed reduction (TPR) and the temperature-programmed oxidation (TPO). Details of these characterizations and experiments are presented in Section 3.

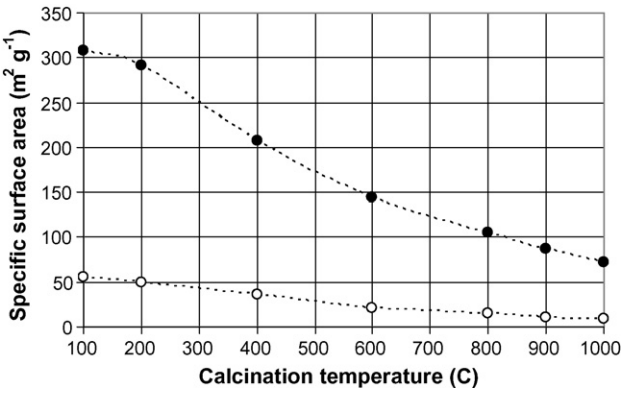

Fig. 1. Specific surface area of CeO_2 (HSA) (●) and CeO_2 (LSA) (◯) after drying and calcinations at different temperatures.

For comparison, conventional Ni/Al_2O_3 (5 wt.% Ni) was also prepared by impregnating α-Al_2O_3 (Aldrich) with $NiCl_3$. After stirring, the solution was dried and calcined for 6 h. The catalyst was also reduced with 10% H_2/He for 6 h before use.

2.2. Apparatus and procedures

An experimental reactor system was constructed as shown in Fig. 2. The feed gases including the components of interest (ethanol and steam from the evaporator) and the carrier gas (helium) were introduced to the reaction section, in which a 10-mm diameter quartz reactor was mounted vertically inside a furnace. The catalyst was loaded in the quartz reactor, which was packed with a small amount of quartz wool to prevent the catalyst from moving.

After the reactions, the exit gas mixture was transferred via trace-heated lines to the analysis section, which consists of a Porapak Q column Shimadzu 14B gas chromatograph (GC) and a mass spectrometer (MS). The gas chromatography was applied in order to investigate the steady state condition experiments, whereas the mass spectrometer in which the sampling of the exit gas was done by a quartz capillary and differential pumping was used for the transient carbon formation experiment. In order to study the formation of carbon species on catalyst surface, temperature-programmed oxidation (TPO) was applied by introducing 10% oxygen in helium into the system, after purged the system with helium. The operating temperature increased from 100 to 1000 °C. The amount of carbon formation on the surface of catalysts was determined by measuring the CO and CO_2 yields from the TPO results. In addition to the TPO method, the amount of carbon deposition was confirmed by the calculation of carbon balance in the system. The amount of carbon deposited on the surface of catalyst would theoretically be equal

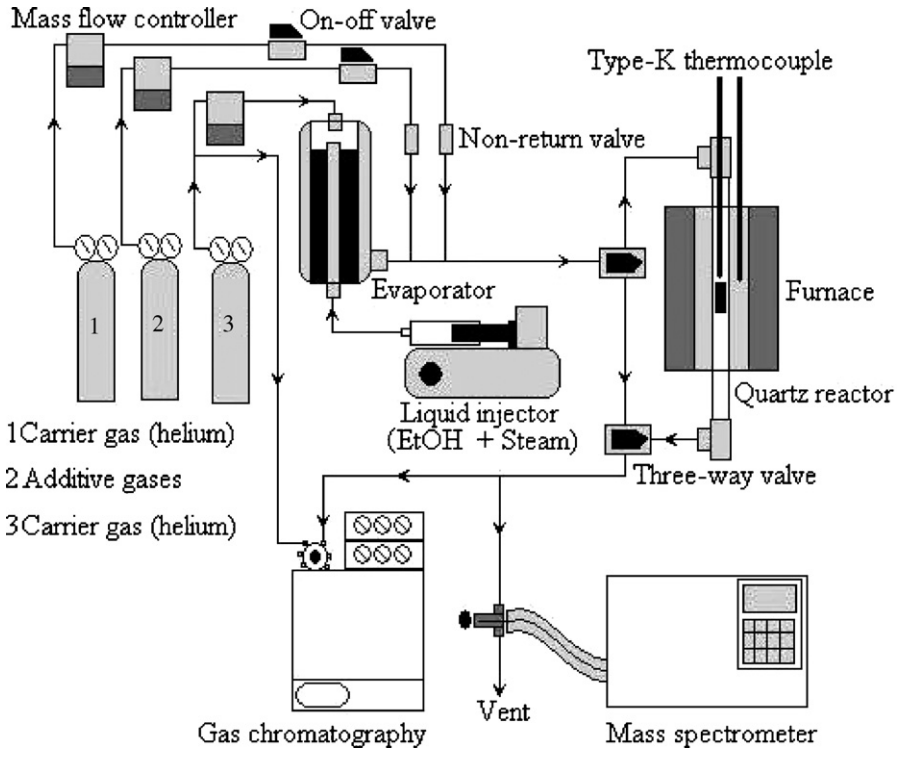

Fig. 2. Schematic diagram of the experimental set-up.

to the difference between the inlet carbon containing components (C_2H_5OH) and the outlet carbon containing components (CO, CO_2, CH_3CHO, C_2H_6, C_2H_4, and CH_4).

The performances of the reforming of ethanol were defined in terms of conversion ($X_{Ethanol}$) and the product selectivities of hydrogen, carbon monoxide, carbon dioxide, methane, ethane, ethylene, and acetaldehyde ($S_{product}$) which are calculated according to Eqs. (1)–(8):

$$X_{Ethanol} = \frac{100(\%Ethanol_{in} - \%Ethanol_{out})}{\%Ethanol_{in}} \quad (1)$$

$$S_{H_2} = \frac{100(\%H_2)}{3(\%Ethanol_{in} - \%Ethanol_{out})} \quad (2)$$

$$S_{CO} = \frac{100(\%CO)}{2(\%Ethanol_{in} - \%Ethanol_{out})} \quad (3)$$

$$S_{CO_2} = \frac{100(\%CO_2)}{2(\%Ethanol_{in} - \%Ethanol_{out})} \quad (4)$$

$$S_{CH_4} = \frac{100(\%CH_4)}{2(\%Ethanol_{in} - \%Ethanol_{out})} \quad (5)$$

$$S_{C_2H_6} = \frac{100(\%C_2H_6)}{(\%Ethanol_{in} - \%Ethanol_{out})} \quad (6)$$

$$S_{C_2H_4} = \frac{100(\%C_2H_4)}{(\%Ethanol_{in} - \%Ethanol_{out})} \quad (7)$$

$$S_{CH_3CHO} = \frac{100(\%CH_3CHO)}{(\%Ethanol_{in} - \%Ethanol_{out})} \quad (8)$$

3. Results

3.1. Redox properties and redox reversibility of the synthesized catalysts

Firstly, the oxygen storage capacities (OSC) and the degree of redox properties for CeO_2 (both LSA and HSA) and Ni/Al_2O_3 were characterized using temperature-programmed reduction (TPR-1), which was performed by heating the reduced catalysts up to 900 °C in 5% H_2 in helium. As shown in Fig. 3, hydrogen consumptions of CeO_2 are detected at the temperature above 650 °C. The amount of hydrogen uptake over CeO_2 (HSA) is significantly higher than that over CeO_2 (LSA), suggesting that the OSC strongly depends on the specific surface area of CeO_2.

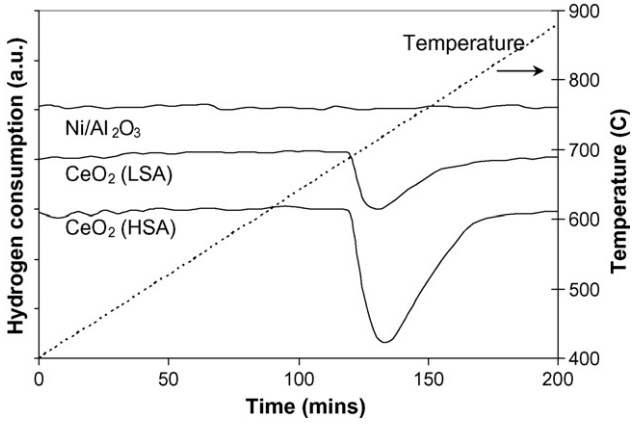

Fig. 3. Temperature-programmed reduction (TPR-1) of fresh catalysts after reduction.

Table 1
Results of TPR-1, TPR-2, and TPR-3, and TPO-1 and TPO-2 for CeO_2 (both HSA and LSA)

Catalyst	Total H_2 uptake from TPR[a] ($\mu mol/g_{cat}$)			Total O_2 uptake from TPO[b] ($\mu mol/g_{cat}$)	
	TPR-1	TPR-2[c]	TPR-3	TPO-1	TPO-2
CeO_2 (HSA)	2159	2155	2158	1044	1047
CeO_2 (LSA)	830	828	830	401	403

[a] Temperature-programmed reduction of the reduced catalysts (relative standard deviation = ±3%).
[b] Temperature-programmed oxidation after TPR-1 (relative standard deviation = ±1%).
[c] Re-temperature-programmed reduction after TPO (relative standard deviation = ±2%).

In contrast, no hydrogen consumption was observed from the TPR over Ni/Al_2O_3, indicating no OSC property for this catalyst.

After purged with helium, the redox reversibility for each catalyst was then determined by applying temperature-programmed oxidation (TPO-1) followed by the second temperature-programmed reduction (TPR-2). Regarding the TPR-2 results, the amount of hydrogen uptakes for CeO_2 (both LSA and HSA) were approximately similar to those from TPR-1, indicating the redox reversibility for these CeO_2. The second temperature-programmed oxidation (TPO-2) and the third temperature-programmed reduction (TPR-3) were also performed in order to reconfirm the redox reversibility. The amounts of oxygen and hydrogen consumptions almost similar to those from TPO-1 and TPR-1 and 2 as presented in Table 1.

3.2. Homogenous (non-catalytic) reaction

Before studying the catalyst performance, homogeneous (non-catalytic) decomposition of ethanol was primarily investigated. Inlet H_2O/C_2H_5OH in helium with the molar ratio of 0.0 (inlet C_2H_5OH of 3.0 kPa) was introduced to the system, while the temperature increased from room temperature to 1000 °C. Fig. 4 shows the product selectivities from the decomposition of ethanol; it was observed that ethanol was converted to acetaldehyde, and hydrogen at the temperature above 200 °C. Methane and carbon dioxide productions were initially observed at the temperature of 250–300 °C. When the temperature increased up to 550 °C, the selectivity of acetaldehyde significantly decreased, while those of hydrogen, carbon monoxide, and carbon dioxide selectivities remained increased. Note that in this range of temperature, the formations of ethane and ethylene were also observed.

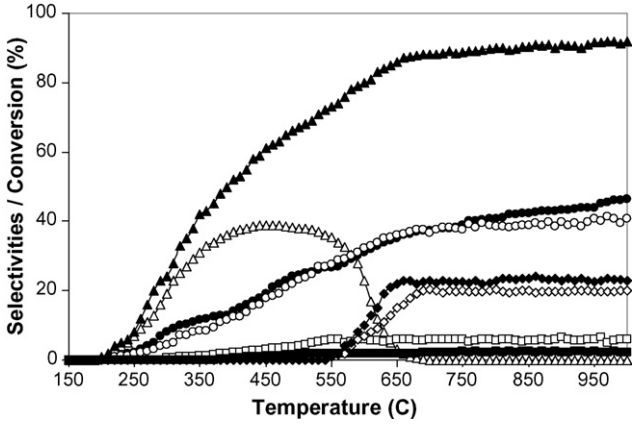

Fig. 4. Homogenous (in the absence of catalyst) reactivity of ethanol decomposition (4 kPa C_2H_5OH) (EtOH (▲), H_2 (●), CO (◯), CO_2 (■), CH_4 (□), CH_3CHO (△), C_2H_6 (◊), and C_2H_4 (♦)).

3.3. Catalytic reactivity toward ethanol decomposition

The decomposition of ethanol with and without steam over CeO_2 (HSA), conventional CeO_2, and Ni/Al_2O_3 were first studied at 900 °C. The feed at different inlet H_2O/C_2H_5OH molar ratios of 0.0, 1.0, and 3.0 (inlet C_2H_5OH of 3.0 kPa) was introduced to the system. The variations in hydrogen selectivity (%) with time at 900 °C over different catalysts and different inlet H_2O/C_2H_5OH ratios are shown in Fig. 5. After operated for 10 h, the hydrogen selectivities for CeO_2 (HSA) were significantly higher than those for conventional CeO_2 and Ni/Al_2O_3; however, the deactivations were also observed for all catalysts. Catalyst stabilities expressed as deactivation percentages are given in Table 2. The post-reaction temperature-programmed oxidation (TPO) experiments over the spent catalysts were then carried out after a helium purge by introducing 5% oxygen in helium in order to determine whether the observed deactivation is due to the carbon formation. From the TPO results shown in

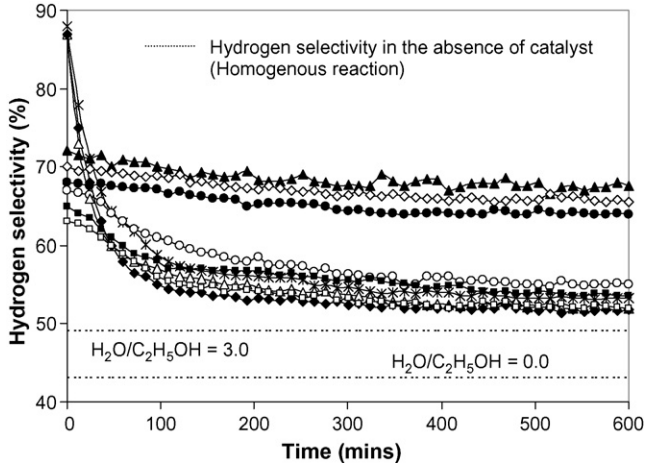

Fig. 5. Decomposition of ethanol (with and without steam) at 900 °C for several catalysts and various inlet H_2O/C_2H_5OH ratios (CeO_2 (HSA) with H_2O/C_2H_5OH of 3.0 (▲), CeO_2 (HSA) with H_2O/C_2H_5OH of 1.0 (◊), CeO_2 (HSA) with H_2O/C_2H_5OH of 0.0 (●), CeO_2 (LSA) with H_2O/C_2H_5OH of 3.0 (◯), CeO_2 (LSA) with H_2O/C_2H_5OH of 1.0 (■), CeO_2 (LSA) with H_2O/C_2H_5OH of 0.0 (□), Ni/Al_2O_3 with H_2O/C_2H_5OH of 3.0 (×), Ni/Al_2O_3 with H_2O/C_2H_5OH of 1.0 (△), and Ni/Al_2O_3 with H_2O/C_2H_5OH of 0.0 (♦).

Table 2
Physicochemical properties of the catalysts after exposure in ethanol decomposition with and without steam at 900 °C for 10 h

Catalyst	C_2H_5OH/H_2O ratio	Yield of H_2 (%) at steady state	Deactivation (%)	BET surface ($m^2\ g^{-1}$)	C formation (monolayers)
CeO_2 (HSA)	1.0/0.0	63.9	6.0	22.6	~0[a] (~0)[b]
	1.0/1.0	65.5	6.4	22.5	0 (0)
	1.0/3.0	67.9	6.1	22.5	0 (0)
CeO_2 (LSA)	1.0/0.0	52.0	18.1	7.2	0.81 (0.80)
	1.0/1.0	53.9	17.6	7.4	0.74 (0.74)
	1.0/3.0	54.5	17.4	7.4	0.67 (0.69)
Ni/Al_2O_3	1.0/0.0	51.8	40.4	39.0	4.64 (4.66)
	1.0/1.0	52.0	40.2	~40.0	4.59 (4.58)
	1.0/3.0	53.2	39.5	~40.0	4.52 (4.54)

Nickel dispersion (measured from temperature-programmed desorption (TPD) after TPR).
[a] Measured from X-ray fluorescence analysis.
[b] Nickel reducibility (measured from temperature-programmed reduction (TPR) with 5% hydrogen).

Fig. 6, the huge amounts of carbon deposition were observed for Ni/Al_2O_3, whereas significantly lower carbon formations were detected for CeO_2 (LSA). No formation of carbon species was detected over CeO_2 (HSA) in all conditions. The values of carbon formations (monolayer) on the surface of catalysts were determined by measuring these CO and CO_2 yields (using Microcal Origin Software). Using a value of 0.026 nm^2 for the area occupied by a carbon atom in a surface monolayer of the basal plane in graphite [25], the quantities of carbon deposited on each catalyst were observed as also presented in Table 2. The total amounts of carbon deposited were then ensured by calculating the carbon balance of the system. Regarding the calculations, for the inlet H_2O/C_2H_5OH ratios of 0.0, 1.0, and 3.0, the moles of carbon deposited per gram of CeO_2 (LSA) were 0.84, 0.79, and 0.73 mmol g^{-1}. By the same assumption for the area occupied by a carbon atom [25], these values are equal to 0.80, 0.74, and 0.69 monolayers, respectively, which are in good agreement with the values observed from the TPO method described above. The results clearly indicated that the deactivations observed for Ni/Al_2O_3 were mainly due to the carbon deposition on the surface of catalyst, and CeO_2 especially the high surface area one presented significantly stronger resistance toward carbon formation compared to Ni/Al_2O_3. The BET measurements were carried out to observe the surface area reduction percentages of all catalysts. As shown in Table 2, it was suggested that the deactivations of ceria are also due to the thermal sintering. Clearly, the surface area reduction percentage of CeO_2 (HSA) is much lower than CeO_2 (LSA), indicating its better stability toward the thermal sintering.

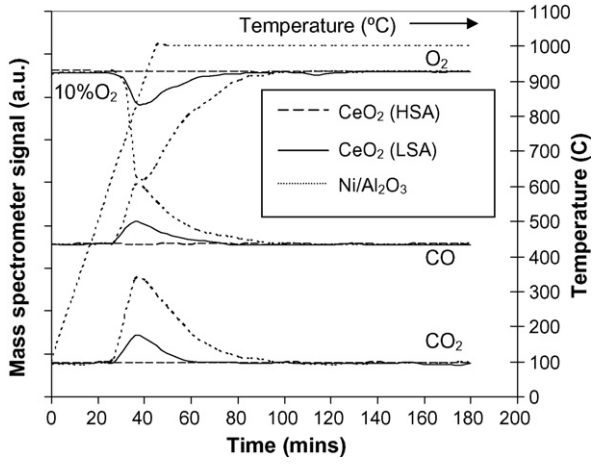

Fig. 6. Temperature-programmed oxidation (TPO) of CeO_2 (HSA), CeO_2 (LSA), and Ni/Al_2O_3 after exposure in the decomposition of ethanol for 10 h (4 kPa C_2H_5OH).

3.4. Effects of temperature and inlet reactants

The influences of operating temperature and the inlet steam content on the product selectivities and ethanol conversion over CeO_2 (both HSA and LSA) were further studied by varying temperature from 700 to 1000 °C and changing the inlet H_2O/C_2H_5OH molar ratios from 0.0 to 1.0, and 3.0, Figs. 7 and 8.

From the study, in the range of temperature between 700 and 850 °C, it was found that H_2, CO, and CH_4 selectivities increased with increasing temperature, whereas C_2H_4, C_2H_6, and CO_2 selectivities decreased. At the temperature above 850 °C, the yield of CH_4 production starts leveling off, which is due to the strong endothermic steam reforming of CH_4 at high temperature. By considering the effect of steam, H_2 and CO_2 selectivities increased with increasing inlet steam concentration, whereas CO selectivity decreased. These are mainly due to the influence of mildly exothermic water–gas shift reaction ($CO + H_2O \rightarrow CO_2 + H_2$). It should be noted that C_2H_4 and C_2H_6 selectivities decreased with increasing temperature and inlet steam content. In addition, compared between CeO_2 (HSA) and CeO_2 (LSA) in Figs. 7 and 8, no formation of C_2H_4 and C_2H_6 was detected at the temperature above 900 °C for CeO_2 (HSA), whereas appreciable amount of C_2H_4 was still observed from the ethanol steam reforming over CeO_2 (LSA) even at 1000 °C.

The ethanol conversions and the product selectivities from the steam reforming of ethanol over both CeO_2 (HSA) and CeO_2 (LSA) were also compared to those values at equilibrium state, which were calculated using AspenPlus10.2 simulation program. As presented in Table 3, according to the simulation, the conversions of ethanol at equilibrium level are 100% in the range of temperature studied, 700–1000 °C. The yields of hydrogen production at equilibrium are higher than those achieved

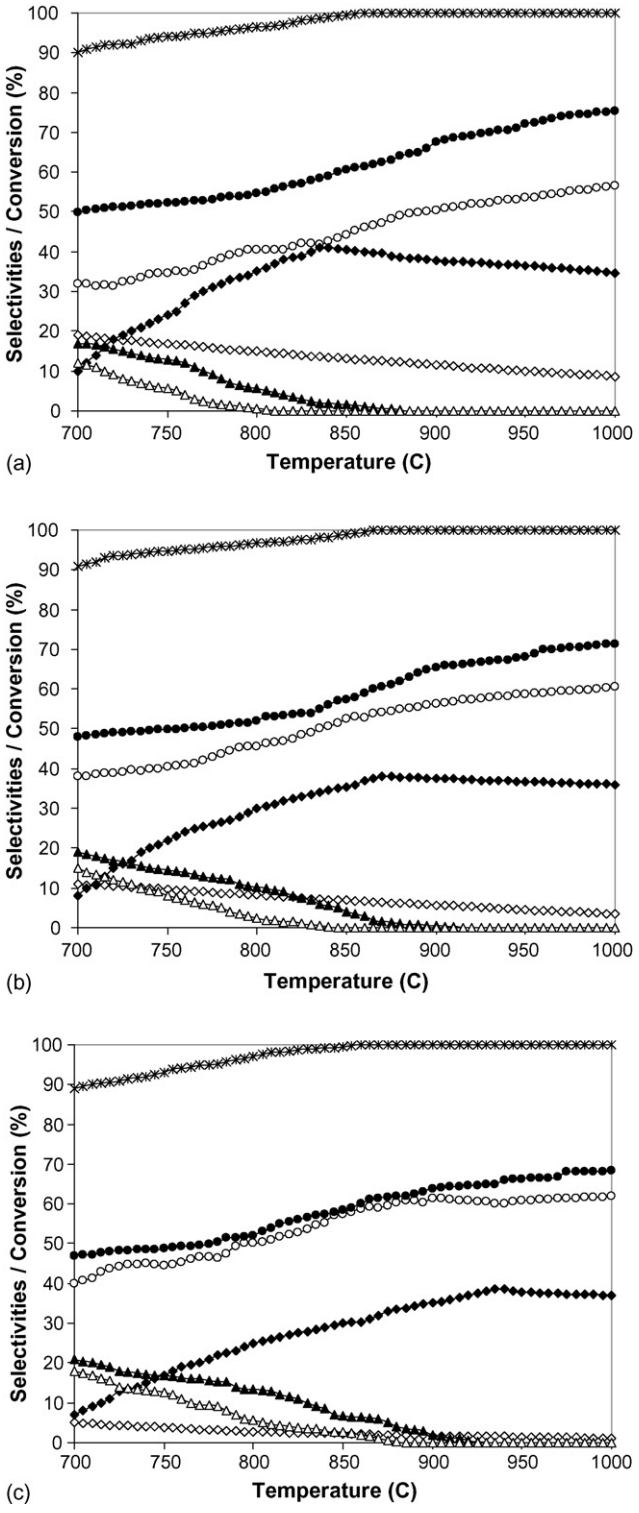

Fig. 7. Effect of temperature on the conversion and product selectivities (EtOH (×), H_2 (●), CO (◯), CO_2 (◊), CH_4 (♦), C_2H_6 (△), and C_2H_4 (▲)) from ethanol steam reforming over CeO_2 (HSA) with H_2O/C_2H_5OH ratios of 3.0 (a), 1.0 (b), and 0.0 (c).

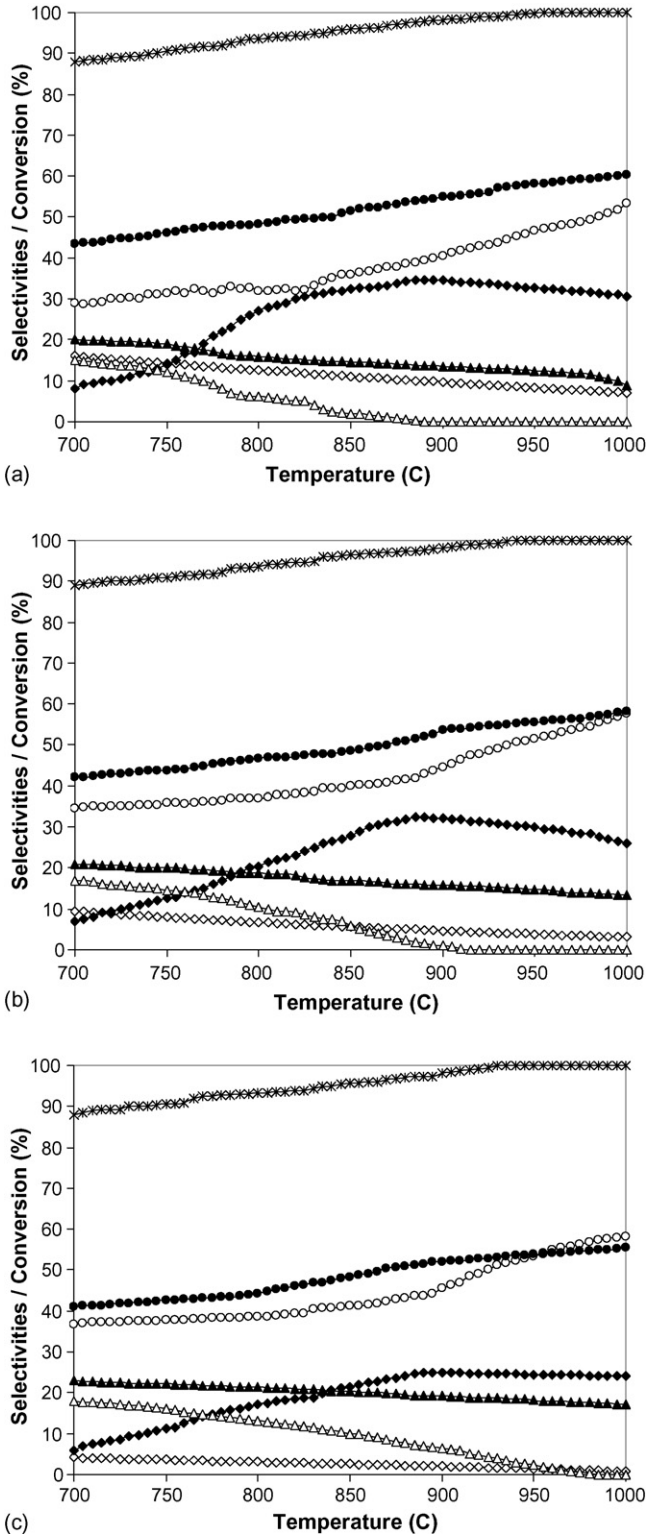

Fig. 8. Effect of temperature on the conversion and product selectivities (EtOH (×), H_2 (●), CO (◯), CO_2 (◊), CH_4 (♦), C_2H_6 (△), and C_2H_4 (▲)) from ethanol steam reforming over CeO_2 (LSA) with H_2O/C_2H_5OH ratios of 3.0 (a), 1.0 (b), and 0.0 (c).

Table 3
Ethanol conversion and the product selectivities from ethanol steam reforming over CeO_2 (HSA) and CeO_2 (LSA) (with the inlet H_2O/C_2H_5OH of 3.0) at 900 °C compared to those from the homogeneous reaction and the equilibrium level at the same conditions

Catalyst	Conversion and product selectivities						
	C_2H_5OH	C_2H_6	C_2H_4	CH_4	H_2	CO	CO_2
CeO_2 (HSA)	100	0	0	37.9	67.9	50.5	11.6
CeO_2 (LSA)	98.1	0	13.5	34.6	54.5	40.3	9.65
Homogeneous	87.6	20.1	21.9	5.9	49.0	30.1	9.6
Equilibrium	100	0	0	0	~100	76.9	23.1

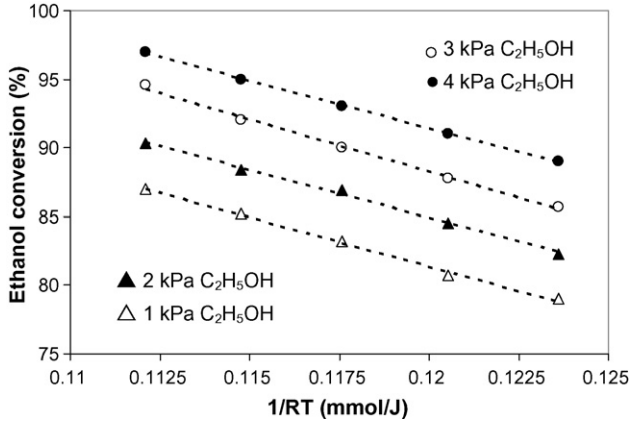

Fig. 9. Arrhenius plot of ethanol conversion from the decomposition of ethanol without steam over CeO_2 (HSA) with different inlet ethanol partial pressures (1–4 kPa) at 700–900 °C.

over CeO_2. In addition, neither C_2H_6 nor C_2H_4 formation was observed in all conditions due to the complete reforming of this component to CH_4, CO, and CO_2.

Without inlet steam, the effect of ethanol concentration on the rate of decomposition over CeO_2 (HSA) was further studied by varying inlet ethanol partial pressure from 1.0 to 4.0 kPa at the temperature between 700 and 900 °C. Fig. 9 presents the Arrhenius plots of the ethanol conversion at various inlet ethanol concentrations. The results show that the conversion of ethanol is proportional to the ethanol concentration and the temperature. Regarding the post-reaction TPO, no carbon formation was observed on the surface of catalysts in all conditions.

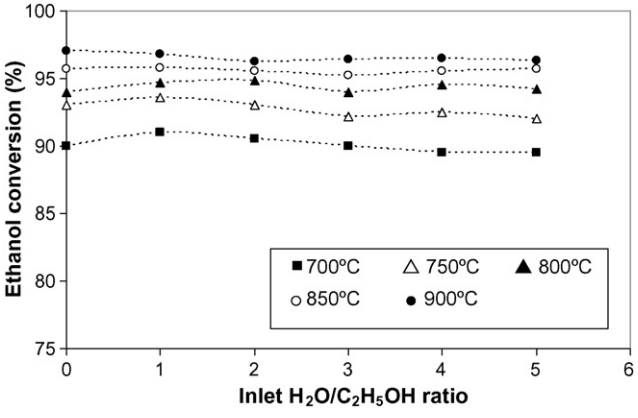

Fig. 10. Effect of steam partial pressure on the conversion of ethanol over CeO_2 (HSA) at different temperatures (4 kPa C_2H_5OH).

In addition, several inlet steam partial pressures were then introduced to the feed with constant ethanol partial pressure in order to investigate the influence of steam on the rate of ethanol decomposition (H_2O/C_2H_5OH of 0.0, 1.0, 2.0, 3.0, 4.0, and 5.0). The ethanol conversion seems to be independent of the inlet steam partial pressure for the range of conditions studied as shown in Fig. 10.

4. Discussion

The decomposition of ethanol at high temperature on the surface of CeO_2 (HSA) can produce H_2, CH_4, CO, and CO_2. This reactivity is due to the presence of the lattice oxygen (O_O^x) in CeO_2, as the hydrocarbons present in the system (i.e. ethanol, ethane, ethylene, and methane) adsorbs and decomposes on the surface of CeO_2 (S_{ce}), and eventually reacts with the lattice oxygen (O_O^x). The gas–solid redox mechanism between these hydrocarbons and the lattice oxygen (O_O^x) on the surface of CeO_2 (HSA) could be derived as illustrated below.

$$C_2H_5OH + 2S_{Ce} = 2(CH_2\text{-}S_{Ce}) + H_2O \quad (9)$$

$$C_2H_6 + 2S_{Ce} = 2(CH_3\text{-}S_{Ce}) \quad (10)$$

$$C_2H_4 + 2S_{Ce} = 2(CH_2\text{-}S_{Ce}) \quad (11)$$

$$CH_4 + 2S_{Ce} = CH_3\text{-}S_{Ce} + H\text{-}S_{Ce} \quad (12)$$

$$CH_3\text{-}S_{Ce} + S_{Ce} = CH_2\text{-}S_{Ce} + H\text{-}S_{Ce} \quad (13)$$

$$CH_2\text{-}S_{Ce} + S_{Ce} = CH\text{-}S_{Ce} + H\text{-}S_{Ce} \quad (14)$$

$$CH\text{-}S_{Ce} + S_{Ce} = C\text{-}S_{Ce} + H\text{-}S_{Ce} \quad (15)$$

$$C\text{-}S_{Ce} + O_O^x = CO + V_O^{\bullet\bullet} + 2e' + S_{Ce} \quad (16)$$

$$2H\text{-}S_{Ce} = H_2 + 2S_{Ce} \quad (17)$$

The lattice oxygen (O_O^x) can be regenerated by the inlet steam and also the steam generated from ethanol dehydration. Normally, the inlet steam is always required during the decomposition of ethanol over a conventional metallic catalyst to prevent the formation of carbon species on catalyst surface. However, it was proven from this study that CeO_2 (HSA) can decompose ethanol efficiently without the presence of inlet steam being required ($H_2O/C_2H_5OH = 0.0$). This could be due to the significant rapid surface reaction of the reduced state CeO_2 with steam generated from the dehydration of ethanol during the decomposition reactions to replenish the lattice oxygen. The strong linear dependence of the inlet ethanol partial pressure and the independence of steam on ethanol decomposition rate also support the idea that the lattice oxygen is replenished by a significant rapid surface reaction of the reduced state CeO_2 with oxygen sources in the system.

Theoretically, the formations of ethylene and ethane are the major difficulties for the catalytic reforming of ethanol, as it has been established that ethane and ethylene act as a very strong promoter of carbon formation. According to the operating temperature in this study (700–1000 °C), carbon formation would

be formed via the decomposition of hydrocarbons and Boudard reactions, Eqs. (18) and (19).

$$C_nH_m = m/2H_2 + nC \quad (18)$$

$$2CO = CO_2 + C \quad (19)$$

By applying CeO_2 (HSA) as the catalyst, the carbon decomposition from both reactions could be inhibited by the gas–solid reactions between gaseous components (ethylene, ethane, and methane produced from the decomposition of ethanol) with the lattice oxygen ($O_O{}^x$) on CeO_2 surface, Eqs. (20) and (21).

$$C_nH_m + O_O{}^x = nCO + m/2H_2 + V_O{}^{\bullet\bullet} + 2e' \quad (20)$$

$$CO + O_O{}^x = 2CO_2 + V_O{}^{\bullet\bullet} + 2e' \quad (21)$$

According to the good performance of CeO_2 (HSA) in terms of high resistance toward carbon deposition and good product selectivities at high temperature, this catalyst would be a good candidate to be applied as the internal or in-stack reforming catalyst for solid oxide fuel cell application (IIR-SOFC), eliminating the requirement of expensive noble metal catalysts or an external pre-reforming installation. In addition, without the inlet steam requirement to decompose ethanol, the consideration of water management in SOFC system can be negligible.

5. Conclusion

High surface area ceria (CeO_2 (HSA)) has useful ethanol decomposition activity producing H_2, CH_4, CO, and CO_2 under solid oxide fuel cells (SOFCs) conditions without the presence of steam being required. The catalyst provides excellent reactivity and high resistance toward carbon deposition compared to Ni/Al_2O_3 and conventional low surface area ceria (CeO_2 (LSA)). These benefits of CeO_2 (HSA) are mainly due to the high redox property of this material.

According to the great benefits of CeO_2 (HSA) in terms of high resistance toward carbon deposition, no inlet steam requirement, and good product selectivities at SOFC temperature, this catalyst would be a good candidate to be applied as the internal or in-stack reforming catalyst (IIR-SOFC).

Acknowledgement

The financial support from The Thailand Research Fund (TRF) throughout this project is gratefully acknowledged.

References

[1] S. Cavallaro, S. Freni, Int. J. Hydrogen Energy 21 (6) (1996) 465–469.
[2] N.F. Athanasio, X.E. Verykios, J. Catal. 225 (4) (2004) 39–452.
[3] L. Garcia, R. French, S. Czernik, E. Chornet, Appl. Catal. A: Gen. 201 (2000) 225.
[4] I. Fishtik, A. Alexander, R. Datta, D. Geana, Int. J. Hydrogen Energy 25 (2000) 31.
[5] S. Freni, G. Maggio, S. Cavallaro, J. Power Sour. 62 (1996) 67.
[6] K. Vasudera, N. Mitra, P. Umasankar, S.C. Dhinga, Int. J. Hydrogen Energy 21 (1996) 13.
[7] S. Cavallaro, S. Freni, Int. J. Hydrogen Energy 21 (1996) 465.
[8] F. Marino, E.G. Cerrella, S. Duhalde, M. Jobbagy, M.A. Laborde, Int. J. Hydrogen Energy 23 (1998) 1095.
[9] S. Cavallaro, Energy Fuels 14 (2000) 1195.
[10] S. Freni, J. Power Sour. 94 (2001) 14.
[11] A. Fatsikostas, D. Kondarides, X. Verykios, Catal. Today 75 (2002) 145.
[12] S. Freni, S. Cavallaro, N. Mondello, L. Spadaro, F. Frusteri, J. Power Sour. 108 (2002) 53.
[13] A. Fatsikostas, D. Kondarides, X. Verykios, Catal. Today 75 (2002) 145.
[14] F. Marino, G. Baronetti, M. Jobbagy, M. Laborde, Appl. Catal. A: Gen. 6043 (2002) 1.
[15] J.P. Breen, R. Burch, H.M. Coleman, Appl. Catal. B: Environ. 39 (2002) 65.
[16] J. Llorca, N. Homs, J. Sales, P. Ramirez de la Piscina, J. Catal. 209 (2002) 306.
[17] V. Fierro, V. Klouz, O. Akdim, C. Mirodatos, Catal. Today 75 (2002) 141.
[18] D. Liguras, D. Kondarides, X. Verykios, Appl. Catal. B: Environ. 43 (2003) 345.
[19] J. Llorca, P. Ramirez de la Piscina, J.-A. Dalmon, J. Sales, N. Homs, Appl. Catal. B: Environ. 43 (2003) 355.
[20] S. Cavallaro, V. Chiodo, S. Freni, N. Mondello, F. Frusteri, Appl. Catal. A: Gen. 249 (2003) 119.
[21] S. Freni, S. Cavallaro, N. Mondello, L. Sadaro, F. Frusteri, Catal. Commun. 4 (2003) 259.
[22] S. Cavallaro, V. Chiodo, A. Vita, S. Freni, J. Power Sour. 123 (2003) 10.
[23] D. Srinivas, C.V.V. Satyanarayana, H.S. Potdar, P. Ratnasamy, Appl. Catal. A: Gen. 243 (2003) 261.
[24] J.R. Rostrup-Nielsen, J.-H. Bak-Hansen, J. Catal. 144 (1993) 38.
[25] E. Ramirez, A. Atkinson, D. Chadwick, Appl. Catal. B 36 (2002) 193–206.
[26] A. Trovareli, C. Leitenburg, G. Dolcetti, Chemtech (1997) 32.
[27] P. Fornasiero, G. Balducci, R.D. Monte, J. Kaspar, V. Sergo, G. Gubitosa, A. Ferrero, M. Graziani, J. Catal. 164 (1996) 173.
[28] T. Miki, T. Ogawa, M. Haneda, N. Kakuta, A. Ueno, S. Tateishi, S. Matsuura, M. Sato, J. Phys. Chem. 94 (1990) 339.
[29] C. Padeste, N.W. Cant, D.L. Trimm, Catal. Lett. 18 (1993) 305.
[30] S. Kacimi, J. Barbier Jr., R. Taha, D. Duperz, Catal. Lett. 22 (1993) 343.
[31] G.S. Zafiris, R.J. Gorte, J. Catal. 143 (1993) 86.
[32] G.S. Zafiris, R.J. Gorte, J. Catal. 139 (1993) 561.
[33] S. Imamura, M. Shono, N. Okamoto, R. Hamada, S. Ishida, Appl. Catal. A 142 (1996) 279.
[34] B.C.H. Steele, P.H. Middleton, R.A. Rudkin, Solid State Ionics 28 (1990) 388.
[35] O.A. Marina, C. Bagger, S. Primdahl, M. Mogensen, in: P. Stevens, U. Bossell (Eds.), Proceedings of the Third European SOFC Forum, Oberrohrdorf, Nantes, Switzerland, 1998, p. 427.
[36] D. Terribile, A. Trovarelli, J. Llorca, C. de Leitenburg, G. Dolcetti, Catal. Today 43 (1998) 79–88.
[37] N. Laosiripojana, S. Assabumrungrat, Appl. Catal. B 60 (1/2) (2005) 107–116.